Tellus (1984), *36A*, 157–165

A noise-free finite element scheme for the two-layer shallow water equations

By BACH-LIEN HUA,[1] *Museum National d'Histoire Naturelle, 43 rue Cuvier, Paris 75005, France,* and FRANCOIS THOMASSET, *Institut National de Recherche en Informatique et en Automatique, Domaine de Voluceau-Rocquencourt, BP 105, Le Chesnay 78150, France*

(Manuscript received July 13, 1982; in final form June 21, 1983)

ABSTRACT

A semi-implicit time marching scheme is combined with triangular finite elements in space for the discretization of the two-layer shallow water equations. Velocity variables are approximated by so-called non-conforming linear elements, which have their nodes at mid-sides of the triangles. Height variables are approximated by linear conforming elements. The resulting discrete scheme is easily inverted and is free of two-grid oscillation problems. It is identical for a particular lattice to a finite difference scheme derived by Mesinger (1973)

1. Introduction

The scheme presented here is motivated by oceanographical applications. In particular, we are concerned with problems where coasts are important and the dynamics can be modelled using the two-layer shallow water equations. The response of the ocean to an impulsive forcing generally has large amplitude near the boundary ("trapped signal") and is strongly dependent upon the coastline geometry. This essential role played by the coastline is a decisive factor in our choice of triangular elements to approximate the coastline geometry.

However, the large number of triangles (around 2000) necessary to map our domain forces us to use linear finite elements on each triangle to appproximate our variables. Linear finite elements have the advantages of simplicity in implementation and savings in core storage space. Furthermore, because of the difference in type of the two variables for which we solve (the two-layer depths h_i ($i = 1, 2$), and the layer velocities $\mathbf{u}_i$), we use different classes of finite elements for each variable. The water heights h_i are approximated by linear conforming elements on each triangle, i.e. are defined at the vertices of the triangles, while the velocities $\mathbf{u}_i$ are defined by so-called non-conforming elements, i.e. are defined at mid-side nodes. Therefore, we have a staggered grid for the distribution of the variables in space (an alternation of h_i and $\mathbf{u}_i$ variables in every grid direction).

For a particular subset of a triangular element grid our scheme is identical to Mesinger's (1973) finite difference scheme for shallow water equations, which was specially devised to remove two-grid oscillations problems in limited area atmosphoric modelling near boundaries.

Furthermore, because of the orthogonality property of the basis of nonconforming linear elements used, the Galerkin discrete form of the shallow water equations at a given node is explicit for the time evolution term. Thus the scheme does not require any contrived "mass-lumping" artifact of the mass matrix and therefore is strictly exact in its discrete formulation.

We check here the accuracy of the scheme against an analytical solution. The scheme has been applied to upwelling problems in the Gulf of Lions (North-West Mediterranean Sea) with satisfactory results (see Hua and Thomasset, 1983).

[1] Present affiliation: The National Center for Atmospheric Research, Boulder, Colorado 80307, U.S.A. (The National Center for Atmospheric Research is sponsored by the National Science Foundation.)

2. Details of the numerical scheme

The shallow water equations that we have to solve (see Hurlburt and O'Brien (1972) for their derivation) are

$$\frac{\partial \mathbf{u}_i}{\partial t} + \overset{A}{[\mathbf{u}_i \cdot \text{grad}]\, \mathbf{u}_i} + \overset{B}{f\mathbf{k} \times \mathbf{u}_i}$$

$$= \overset{C}{-g\, \text{grad}\,(h_1 + h_2 + D)}$$

$$\overset{D}{- g\, \delta_{i2} \frac{\rho_2 - \rho_1}{\rho_0} \text{grad}\, h_1} + \overset{E}{\nu\, \Delta \mathbf{u}_i}$$

$$+ \overset{F}{(\boldsymbol{\tau}_{si} - \boldsymbol{\tau}_{bi})/\rho_0 h_i} \quad (1)$$

$$\frac{\partial h_i}{\partial t} + \overset{G}{h_i \,\text{div}\, \mathbf{u}_i} + \overset{H}{[\mathbf{u}_i \cdot \text{grad}]\, h_i} = 0. \quad (2)$$

The variables we have to solve for are the velocity $\mathbf{u}_i$ and thickness h_i of each layer $i = 1, 2$. $\mathbf{k}$ is the unit vector along the upward local vertical, f is the Coriolis parmeter, ρ_i is the density in each layer $i = 1, 2$, ρ_0 is taken as 10^3 M.K.S., i.e. we have made the Boussinesq approximation. $D(x, y)$ is the bottom topography height above the level surface lying at the bottom of the second layer, and ν is the lateral diffusion coefficient. $\boldsymbol{\tau}_{si}$ is the stress at the surface of each layer, i.e. the wind-stress at the surface of the top layer and the interfacial stress at the top of the bottom layer, and $\boldsymbol{\tau}_{bi}$ is the bottom stress at the bottom of each layer. In practical applications, the stresses will be computed from the usual quadratic laws using wind-speed at 10 m for the wind-stress term and the fluid velocities for interfacial and bottom stress (see Hurlburt and O'Brien (1972) for details). However in the analytical case considered later on, the interfacial and bottom stresses will be set to zero and an analytical form will be chosen for the wind stress.

2.1. *Time discretization*

Because of the presence of external and internal gravity waves, which have phase speeds of propagation of quite different orders of magnitude, a semi-implicit scheme is used for the treatment of the gravity waves terms (C, D, G) while the remaining terms are treated explicitly (Kwizak and Robert, 1971; Hurlburt and O'Brien, 1972), allowing larger time steps.

The terms A, B, F and H are treated explicitly using the leap-frog scheme.

We have for $i = 1, 2$

$$\begin{pmatrix} \mathbf{u}_i \\ h_i \end{pmatrix}^{m+1} = \begin{pmatrix} \mathbf{u}_i \\ h_i \end{pmatrix}^{m-1} + 2\Delta t \begin{pmatrix} A, B, F \\ H \end{pmatrix}^{m}. \quad (3)$$

The lateral diffusion term is treated explicitly with a Euler type scheme (and will thereby limit our time step):

$$\mathbf{u}_i^{m+1} = \mathbf{u}_i^{m-1} + 2\Delta t\, E^{m-1}. \quad (4)$$

The gravity waves terms are first split into non-linear and linear parts by writing

$$h_1(x, y, t) = H_1 + h_1'(x, y, t)$$

$$h_2(x, y, t) = H_2 - D(x, y) + h_2'(x, y, t), \quad (5)$$

where H_1 and H_2 are constants and H_1 (resp. $H - D(x, y)$) is the time-mean depths of layer 1 (resp. 2) and h_i' represents the fluctuations in the thickness of each layer, $i = 1, 2$. h_i' is supposed to remain small compared to the initial values of the layer's thickness h_i, justifying the linearization. Although the topography term $D(x, y)$ is kept through the derivation of the scheme, the analytical case considered deals with a flat bottom. Thus the linear gravity terms are:

$$\frac{\partial \mathbf{u}_i}{\partial_t} = -g\, \text{grad}\,(\alpha_i h_1' + h_2'), \quad i = 1, 2 \quad (6)$$

$$\frac{\partial h_1'}{\partial t} + H_1 \,\text{div}\, \mathbf{u}_1 = 0 \quad (7)$$

$$\frac{\partial h_2'}{\partial t} + (H_2 - D)\, \text{div}\, \mathbf{u}_2 = 0 \quad (8)$$

$$\alpha_1 = 1$$
$$\alpha_2 = 1 - (\rho_2 - \rho_1)/\rho_0. \quad (9)$$

The above terms are discretized using an implicit trapezoidal scheme:

$$\mathbf{u}_i^{m+1} - \mathbf{u}_i^{m-1} = -2g\, \Delta t\, [\tfrac{1}{2} \text{grad}\,(\alpha_i h_1' + h_2')^{m+1} + \tfrac{1}{2} \text{grad}\,(\alpha_i h_1' + h_2')^{m-1}] \quad (10)$$

$$h_1'^{\,m+1} - h_1'^{\,m-1} = 2\Delta t H_1 [\tfrac{1}{2}(\text{div}\, \mathbf{u}_1^{m+1}) + \tfrac{1}{2}(\text{div}\, \mathbf{u}_1^{m-1})]$$

$$h_2'^{\,m+1} - h_2'^{\,m-1} = -2\Delta t (H_2 - D)\, [\tfrac{1}{2}(\text{div}\, \mathbf{u}_2^{m+1}) + \tfrac{1}{2}(\text{div}\, \mathbf{u}_2^{m-1})]. \quad (11)$$

This trapezoidal scheme has neutral temporal stability. However, when one uses this temporal scheme on gravity waves with a centred spatial scheme, the numerical phase speed is slower than the theoretical one for any time step thereby limiting the actual time step value.

For $m > 1$, the final system can be written as:

$$\mathbf{u}_l^{m+1} + g\,\Delta t\,\mathrm{grad}\,(\alpha_l\,h_1'^{\,m+1} + h_2'^{\,m+1}) = \mathbf{v}_l^m \tag{12}$$

$$h_l'^{\,m+1} + \Delta t\,\mathrm{div}\,(\mathscr{H}_l\,\mathbf{u}_l^{m+1}) = k_l^m \tag{13}$$

$$\mathscr{H}_1 = H_1$$

$$\mathscr{H}_2 = H_2 - D(x, y) \tag{14}$$

$$\begin{aligned}\mathbf{v}_l^m = \mathbf{u}_l^{m-1} - 2\Delta t[\tfrac{1}{2}g\,\mathrm{grad}\,(\alpha_l\,h_1'^{\,m-1} + h_2'^{\,m-1}) \\ - \nu\Delta u_l^{m-1} + (\mathbf{u}_l^m\cdot\mathrm{grad})\,\mathbf{u}_l^m + f\mathbf{k}\times\mathbf{u}_l^m \\ - (\tau_{sl} - \tau_{bl})/\rho_0\,h_l^m]\end{aligned} \tag{15}$$

$$k_l^m = h_l'^{\,m-1} - 2\Delta t[\tfrac{1}{2}\,\mathrm{div}\,(\mathscr{H}_l\,\mathbf{u}_l^{m-1}) + \mathrm{div}\,(h_l'\,\mathbf{u}_l^m)]. \tag{16}$$

For the first time step $m = 1$, the integration is started using a Euler scheme of step Δt.

2.2. *Spatial discretization*

It is a common feature of the finite element treatment of shallow water equations that small-scale noise is produced by the spatial discretization, when both variables (h_l and u_l) are approximated identically.

Mesinger and Arakawa (1976) give a review of the solutions found for finite difference schemes. The finite elements case has been analysed by Shoenstadt (1980) and Williams (1981), for one-dimensional meshes. Their conclusion is either to stagger the variables for the shallow water equations variables or to use vorticity/divergence instead of velocity components. We choose here the first solution, i.e. the scalar quantities (water heights) are evaluated at the vertices of the triangle (usual hat function, Fig. 1a) while the vector quantities are evaluated at mid-sides of the triangles, using so-called nonconforming elements (Fig. 1b). We give a short description of non-conforming elements below.

The basis function $w_M(x, y)$ associated with mid-side node M of coordinates x_M, y_M is shown in Fig. 1b. We have

$$\begin{aligned} &w_M(x_M, y_M) = 1 \\ &w_M(x_{M'}, y_{M'}) = 0 \quad \text{if } M \neq M'. \end{aligned} \tag{17}$$

We can see from Fig. 1b the origin of the term "non-conforming" elements: the basis function is discontinuous along the triangle side S_1S_2 (and along S_2S_3, S_1S_4 and S_3S_4 as well). A discussion of their properties can be found in Thomasset (1981).

The most useful property is their orthogonality property:

$$\int_\Omega w_M(x, y)\,w_{M'}(x, y)\,\mathrm{d}x\,\mathrm{d}y = A_M\,\delta_{MM'}/3 \tag{18}$$

where Ω is the domain of integration and A_M is the area of the support of w_M, i.e., the area of the

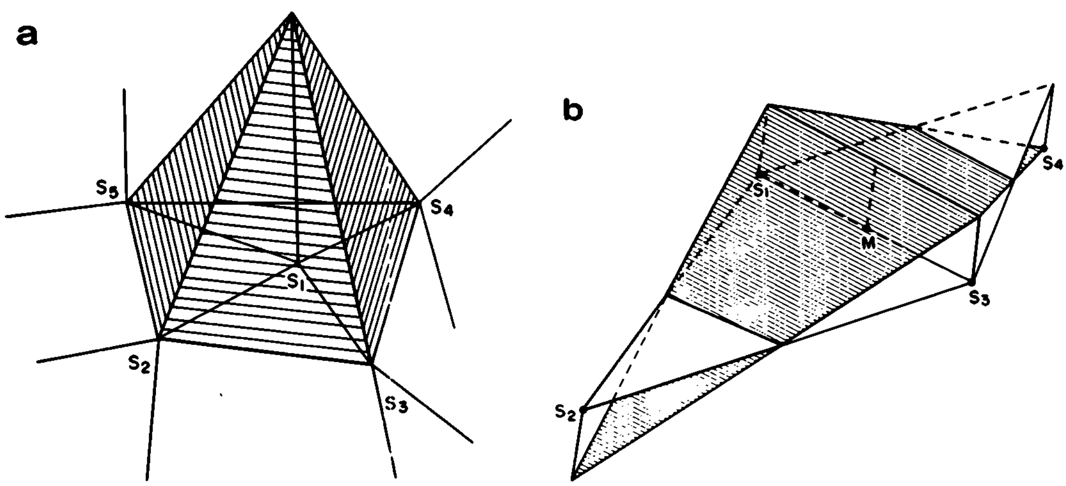

Fig. 1. Shape of a linear basis function (a) for a vertex node S_1. It is zero outside the support triangles $S_1S_2S_3$, $S_1S_3S_4$, $S_1S_4S_5$, $S_1S_5S_2$ and is continuous everywhere; (b) for a mid-side node M. It is zero outside the two support triangles $S_1S_2S_3$ and $S_1S_3S_4$ and is discontinuous along sides S_1S_2, S_2S_3, S_3S_4 and S_1S_4.

triangle $S_1S_2S_3$ and $S_1S_3S_4$ and δ_{ij} is the Kronecker delta. We also have

$$\int_\Omega w_M(x,y)\,dx\,dy = A_M/3. \tag{19}$$

This class of non-conforming elements thus presents several advantages over the usual conforming linear elements defined at the vertices of the triangles. Their Galerkin formulation is no longer implicit in nature and therefore does not require any lumping of the mass matrix, such as commonly done when using conforming elements. For a domain which has a large number of triangles, it is easy to verify that if NM designates the number of mid-side nodes and NS the number of vertices of the triangulation, one has $NM \sim 3NS$. Thus the number of mid-sides variables can be penalizing in terms of core storage space, by comparison with the number of vertices variables. However, the use of conforming elements with the mass lumping approximation, which yields a diagonal matrix, is known to produce disastrous effects on the phase error for highly transient problems.

Since the grid points are located at the mid-side of each triangle, for boundary nodes, the direction of the normal to the boundary is defined without ambiguity and therefore circumvents the difficulty of satisfying exactly the no-normal flux condition at every boundary vertex (Pinder and Gray, 1977), a problem encountered with usual conforming elements. It is important in our problem to satisfy as exactly as possible the boundary condition, since we anticipate that the solution will be strongly trapped near the coast through Kelvin wave-like dynamics. This last remark also explains why we choose to approximate the velocity variables rather than the heights variables by nonconforming elements.

2.2.1. *Velocity variables*. For a general point (x,y) of the domain Ω, one has for each layer $i = 1, 2$

$$\mathbf{u}_i(x,y,t) = \sum_{p\in \mathscr{S}_0} \mathbf{u}_{ip}(t)\, w_p(x,y) + \sum_{p\in \mathscr{S}_1} s_{ip}\, \mathbf{t}_p\, w_p \tag{20}$$

where $\mathscr{S}_0$ is the set of interior mid-side nodes of Ω such that at a given interior mid-node $\mathbf{u}_{ip}(t)$ gives the value of the velocity in layer i at that node and $\mathscr{S}_1$ is the set of mid-side nodes located on the boundary, such that $s_{ip} = \mathbf{u}_i \cdot \mathbf{t}_p \neq 0$ (slip boundary conditions) where $\mathbf{t}_p$ designates the local tangential vector of the boundary. Boundary nodes where there is a no-slip boundary condition do not correspond to degrees of freedom. At a node $p \in \mathscr{S}_1$, because of the no normal flux boundary condition, one has only one degree of freedom of the velocity field.

2.2.2. *Water height displacements* h_i'. Let ϕ_r designate the usual chapeau function basis of piecewise linear elements with degrees of freedom located at the vertices of the triangles. One can expand the water height displacements h_i' as

$$h_i'(x,y,t) = \sum_{r\in \mathscr{S}} h_{ir}'(t)\,\phi_r(x,y) \tag{21}$$

where $\mathscr{S}$ is the set of vertices of the triangles in Ω.

Therefore $h_{ir}'(t)$ gives the water height displacements in each layer at the location of the vertex r. We define S_{rq} as

$$S_{rq} = \int_\Omega \phi_r(x,y)\,\phi_q(x,y)\,dx\,dy. \tag{22}$$

2.2.3. *Discrete system of shallow water equations*. The Galerkin expansion of eqs. (12) yields for an interior mid-side node $P \in \mathscr{S}_0$

$$\overbrace{A_p\,\mathbf{u}_{ip}^{m+1}}^{\text{“evolution term”}} + g\,\Delta t \sum_{q\in \mathscr{S}} (\alpha_i h_{1q}'^{\,m+1} + h_{2q}'^{\,m+1}) \times (\text{grad}\,\phi_q, w_p) = (\mathbf{v}_i^m, w_p) \tag{23}$$

where (,) designates the L^2 scalar product on Ω.

For a boundary node such as $p \in \mathscr{S}_1$

$$A_p s_{ip}^{m+1} + g\,\Delta t \sum_{q\in \mathscr{S}} (\alpha_i h_{1q}'^{\,m+1} + h_{2q}'^{\,m+1}) \times (\mathbf{t}_p \cdot \text{grad}\,\phi_q, w_p) = \mathbf{t}_p \cdot (\mathbf{v}_i^m, w_p). \tag{24}$$

The Galerkin expansion of the continuity eq. (13) yields:

$$\underbrace{S_{rr} h_{ir}'^{\,m+1} + \sum_{q\in \mathscr{V}(r)} S_{rq} h_{iq}'^{\,m+1}}_{\text{“evolution term”}} - \Delta t \sum_{p\in \mathscr{S}_0} \times [\mathbf{u}_{ip}^{m+1} \cdot (\mathscr{H}_i w_p, \text{grad}\,\phi_r)] - \Delta t \sum_{p\in \mathscr{S}_1} \times [s_{ip}^{m+1}\,\mathbf{t}_p \cdot (\mathscr{H}_i w_p, \text{grad}\,\phi_r)] = (k_i^m, \phi_r) \tag{25}$$

where $\mathscr{V}(r)$ is the set of vertices which are distinct from r but still belong to the support of ϕ_r, i.e. for which r is a first neighbour vertex.

The expression for the time evolution term in (23) shows the time-explicit nature of the momentum equations, due to the orthogonality property of the non-conforming elements used for the velocity variables. Eq. (25) illustrates the implicit nature of the usual conforming elements used for the height variables.

2.3. *Structure of the Helmholtz equations*

It is straightforward to take advantage of the explicit nature of the evolution term in (23) to eliminate the velocity variables between (23)–(25), obtaining the following system

$$\left(S_{rr} h'^{m+1}_{lr} + \sum_{q\in \mathcal{T}(r)} S_{rq} h'^{m+1}_{lq}\right) + g\,\Delta t^2 \left[\sum_{q\in\mathcal{S}} \times (\alpha_l h'^{m+1}_{1q} + h'^{m+1}_{2q})\, a^{(l)}_{qr}\right] = f^m_{lr} \tag{26}$$

where the matrix $a^{(l)}_{qr}$ is given by

$$a^{(l)}_{qr} = \sum_{p\in \mathcal{T}_0} A_p^{-1}[(\mathcal{H}_l w_p, \text{grad}\,\phi_r)\cdot(w_p, \text{grad}\,\phi_q)] + \sum_{p\in\mathcal{T}_1} A_p^{-1}[(\mathcal{H}_l w_p, \text{grad}\,\phi_r\cdot t_p) \times (w_p, \text{grad}\,\phi_q\cdot t_p)]. \tag{27}$$

$a^{(l)}_{qr}$ is independent of time and just depends on the grid geometry and therefore needs to be assembled just once. In the case of a flat bottom, one can factorise $\mathcal{H}_l$. One can see that $a^{(l)}_{qr}/\mathcal{H}_l$ is the analogue of a discretized form of a Laplacian operator so that (26) is analogous to a discretized Helmholtz equation for the two-layer case

$$h'_i + g\,\Delta t^2 \mathcal{H}_l\,\Delta(\alpha_l h'_1 + h'_2) = 0 \quad \text{for i} = 1, 2. \tag{28}$$

However, one should note that (26) is not the discrete Galerkin form of (28), when replacing directly the h'_l variables by their basis expansion (21).

The right-hand side of (26) is given by

$$f^m_{lr} = (k^m_l, \phi_r) + \Delta t \sum_{p\in\mathcal{T}_0} A_p^{-1}[(\mathcal{H}_l w_p, \text{grad}\,\phi_r)\cdot (\mathbf{v}^m_l, w_p) + \Delta t \sum_{p\in\mathcal{T}_1} A_p^{-1}\,[(\mathcal{H}_l w_p, \text{grad}\,\phi_r\cdot t_p) \times (w_p, \mathbf{v}^m_l\cdot t_p)]. \tag{29}$$

At each time step we have to solve the system (26) and (27) in order to obtain the heights h'_l.

The system can be rewritten as:

$$\begin{pmatrix} B_{11}\cdots B_{1r}\cdots & & \cdots \\ \vdots & \vdots & \\ B_{r1}\cdots B_{rr}\cdots B_{rq}\cdots & & \\ \vdots & \vdots & \\ \vdots & \vdots & \end{pmatrix} \begin{pmatrix} h'_{11} \\ h'_{21} \\ \vdots \\ h'_{1r} \\ h'_{2r} \\ \vdots \\ \vdots \end{pmatrix} = \begin{pmatrix} f_{11} \\ f_{21} \\ \vdots \\ \vdots \\ \vdots \\ f_{1q} \\ f_{2q} \\ \vdots \end{pmatrix} \tag{30}$$

where each block B_{rq} is defined by:

$$B_{rq} = \begin{pmatrix} g\,\Delta t^2 a^{(1)}_{rq} + S_{rq} & g\,\Delta t^2 a^{(1)}_{rq} \\ g\,\Delta t^2 a^{(2)}_{rq}\,\alpha_2 & g\,\Delta t^2 a^{(2)}_{rq} + S_{rq} \end{pmatrix} \tag{31}$$

and $a^{(l)}_{rq}$ is given by (27).

B_{rq} differs from zero only when q is a vertex which is either a direct neighbour of r or a first indirect neighbour of r. The matrix that one has to invert in (29) is therefore a very sparse block-matrix and we only need to store the blocks that are different from zero.

Eq. (29) is inverted by a Block Successive Over-Relaxation method, n being the iteration number and ω the relaxation parameter. One has

$$\begin{pmatrix} h'_{1r} \\ h'_{2r} \end{pmatrix}^{(n+1)} = (1-\omega)\begin{pmatrix} h'_{1r} \\ h'_{2r} \end{pmatrix}^{(n)} - \omega[B_{rr}]^{-1}\left\{\sum_{q=1}^{r-1} B_{rq}\begin{pmatrix} h'_{1q} \\ h'_{2q} \end{pmatrix}^{(n+1)} + \sum_{q=r+1}^{NS} B_{rq}\begin{pmatrix} h'_{1q} \\ h'_{2q} \end{pmatrix}^{(n)} - \begin{pmatrix} f_{1r} \\ f_{2r} \end{pmatrix}\right\}. \tag{32}$$

This block S.O.R. method is chosen because it converges more rapidly than a point S.O.R. method. Moreover it requires less core storage space than a direct method such as a Cholesky decomposition.

Once the new water height displacements h'^{m+1}_{lq} have been obtained at time step $m + 1$, the values of the velocity field $\mathbf{u}^{m+1}_{ul}$ are calculated explicitly from (23).

2.4. *Finite difference analogue*

The motivation for this paragraph is to look for an analogue of our finite element scheme among the existing finite differences schemes. It should however be kept in mind that we are using triangular elements and not rectangular ones, so that a one-to-one correspondence will not be found with rectangular finite differences meshes for all directions of the grid.

The closest scheme is a finite difference one devised by Mesinger (1973), using centred differences on an (E) lattice. The scheme involves the introduction of auxiliary velocity points along the *diagonal* directions of the grid, midway between the neighbouring height points (points noted by 5, 6, 7, 8 on Fig. 2). Velocity components at these points are assumed to have space-averaged values and are used for a more accurate calculation of the divergence term in the continuity equation. The modification procedure makes a single grid point height perturbation propagate as a gravity wave along all height points of the grid. Since a velocity perturbation can propagate as a gravity wave only through excitation of height perturbations, the method is sufficient to prevent the false two-grid interval noise in all of the dependent variables, at least as long as *non-linear* spurious energy cascade does not occur, such as documented in Arakawa and Lamb (1981, p. 27), even for a staggered grid.

If we use the triangular finite element grid of Fig. 3, where solid lines now delineate the triangular elements used for heights and velocity variables, it can be readily verified that our Laplacian operator $a_{qr}^{(i)}/\mathscr{K}_i$ gives the following interaction coefficients between height variable h_0 and its neighbours:

$$a_{00} = 12\gamma$$

$$a_{01} = a_{02} = a_{03} = a_{04} = -\gamma \tag{33}$$

$$a_{05} = a_{06} = a_{07} = a_{08} = -2\gamma$$

where $\gamma = 1/4d^2$ is a factor depending on the grid dimensions (Figs. 2 and 3). This yields the following Laplacian discretization

$$\Delta h_0 = \frac{1}{4d^2}\,[h_1 + h_2 + h_3 + h_4 + 2(h_5 + h_6 + h_7 + h_8) - 12h_0] \tag{34}$$

which has exactly the same weighting as the one obtained by Mesinger's scheme for the height variable h_0.

However, a finite difference rectangular grid behaves inhomogeneously from a triangular finite element point of view. As can be seen from Fig. 4, while h_0 has a support of four triangles, h_8 has a support of eight triangles. Our Laplacian operator $a_{qr}^{(i)}/\mathscr{K}_i$ centred on h_8 would give the following 13 points Laplacian discretization:

$$\Delta h_8 = \frac{1}{d^2}\,[(h_5 + h_7 + h_{13} + h_{14}] + 2(h_0 + h_1 + h_4 + h_{14}) + (h_6 + h_{10} + h_{11} + h_{12}) - 16h_8)]. \tag{35}$$

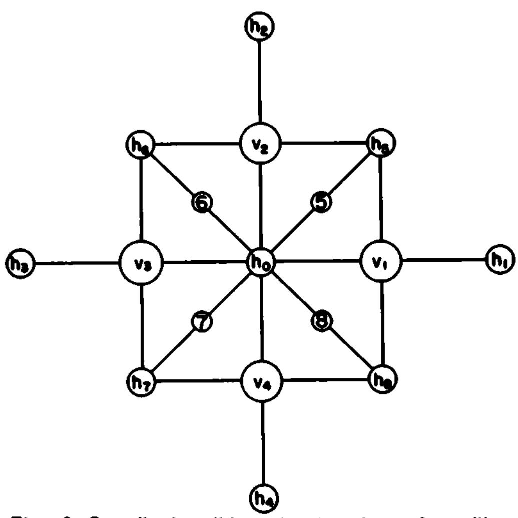

Fig. 2. Stencil describing the location of auxiliary velocity variables used for the construction of Mesinger's scheme.

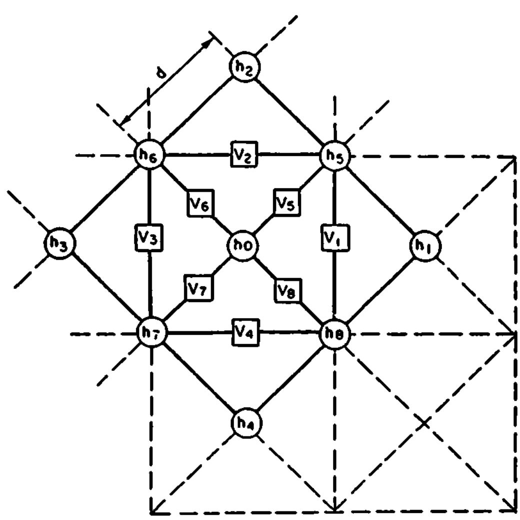

Fig. 3. Finite element grid centred around h_0 corresponding to Mesinger's scheme.

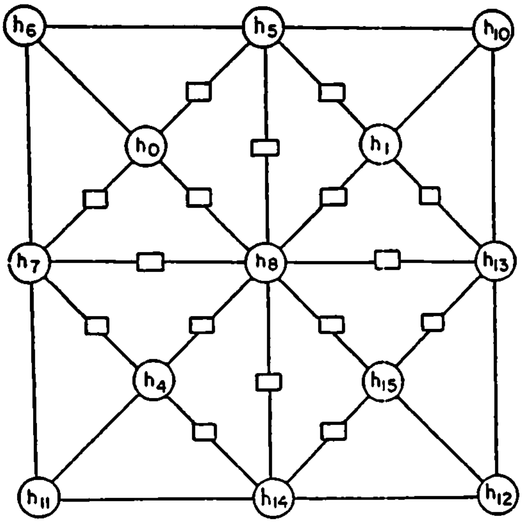

Fig. 4. Finite element grid centred around h_8 used for describing (35).

Platzman (1981) has showed that an inhomogeneous triangulation would cause small-scale noise and the best results will be obtained from a grid composed of equilateral triangles (Fig. 5), which is invariant with respect to translation and rotation. For such a grid, the truncation error on the discretized Laplacian which is

$$\Delta h_0 = \frac{4}{3d^2} [\tfrac{1}{2}(h_1 + h_2 + \ldots + h_6) + \tfrac{1}{6}(h_7 + \ldots + h_{12}) - 4h_0] \quad (36)$$

will be the same for all nodes.

We mainly compared our scheme (below referred to as scheme A) for given triangular grids to another finite element scheme (scheme B) which uses non-conforming triangular elements for both height and velocity variables (both variables are chosen at mid-side nodes of the triangles), retaining a semi-implicit scheme in time.

Scheme B showed spurious noise at two-grid interval spaces for all variables near the boundaries of our domain, while at the same node locations, scheme A showed no such noise for velocity variables (at least to a relative precision of 1% in velocity components). At the same precision no noise was indicated for the vertex height variables. Apart from the linear argument of two-grid interval noise prevention given earlier, the absence of noise on the velocity variables due to a non-linear energy

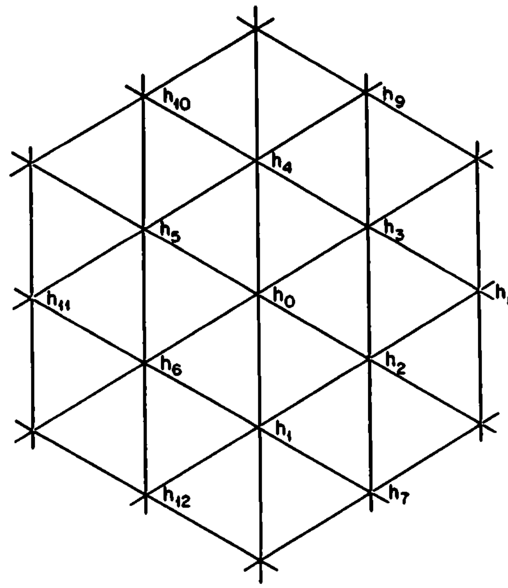

Fig. 5. Homogeneous finite element grid centred around h_0 and used for describing (36).

cascade might be due to a fact mentioned by Mesinger (1973), that the finite difference analogue of scheme A used with an implicit time scheme damps shorter waves to some extent (as does the non-modified implicit scheme using centred differences on lattice (E)).

3. A simple test case

We have tested our scheme for a simple case for which Crepon and Richez (1982) have provided us with an analytical solution. It corresponds to the following values of the parameters of eqs. (1, 2): $\nu = 0$, $\tau_{b1} = \tau_{b2} = \tau_{s2} = 0$, $D(x, y) = 0$. The wind-stress τ_{s1} (hereafter denoted simple τ) is chosen as

$$\begin{aligned} \tau_x &= 0 && \text{for } |y| > b \\ \tau_y &= \tau_0(1 - |y|/b)\, H(t) && \text{for } |y| < b \end{aligned} \quad (37)$$

where x is the cross shore direction, y is the alongshore direction, and $H(t)$ is the Heaviside function. The wind-stress therefore only acts on a strip perpendicular to the coastline. The two layers are initially at rest and the wind-stress is switched on at $t = 0$.

After the decay of inertial oscillation terms like $\sin(ft)/\sqrt{ft}$, the interface displacement h_2' is given by the following expression (when neglecting terms of order less than $[(\rho_2 - \rho_1/\rho_0) H_1 H_2/(H_1 + H_2)^2]^{1/2}$:

for $b < y$ $\quad h_2' = 0$;

for $0 < y < b$

$$h_2' = \frac{H_2}{H_1 + H_2} \frac{\tau_0}{2\rho_0 b} \exp \left\{ -xf/c \left[(t + (y-b)/c)^2 \times H(ct + y - b) - t^2 - 2\frac{(y-b)\,t}{c} \right] \right\}; \quad (38)$$

for $-b < y < 0$

$$h_2' = \frac{H_2}{H_1 + H_2} \frac{\tau_0}{2\rho_0 b} \exp \left\{ -xf/c \left[(t + (y-b)/c)^2 \times H(ct + y - b) - 2(t + y/c)^2 H(ct + y) + t^2 + 2\frac{(y+b)\,t}{c} \right] \right\};$$

for $y < -b$

$$h_2' = \frac{H_2}{H_1 + H_2} \frac{\tau_0}{2\rho_0 b} \exp \{ -xf/c[(t + (y-b)/c)^2 \times H(ct + y - b) - 2(t + y/c)^2 H(ct + y) + (t + (y+b)/c)^2 H(ct + y + b)] \};$$

$$c_2 = g(\rho_2 - \rho_1)/\rho_0 \frac{H_1 H_2}{H_1 + H_2}.$$

Thus the response consists of the excitation of three Kelvin wave fronts at points $y = b$, $y = 0$, $y = -b$, whose amplitudes partly cancel as they propagate towards $y < 0$. Eq. (38) can be readily deduced from the solution documented in Crepon and Richez (1982, p. 1444), or by using the method of characteristics as in Allen (1976), since our case corresponds to a continuous wind-stress which, inside the strip $|y| < b$, is a linear function of y while their case corresponds to a constant value. Right at the coast the inertial oscillations terms in $\sin(ft)$ are identically zero, so that (38) is valid from the beginning of the time integration.

The simulation corresponds to $H_1 = 50$ m, $H_2 = 200$ m, $\rho_2 - \rho_1/\rho_0 = 4 \cdot 10^{-3}$, $f = \sqrt{2}\ 10^{-4}$ sec^{-1}, $b = 50$ km. The time step is such that $f\Delta t = 0.05$, the alongshore grid dimension is $\Delta y/b = 0.2$ and we use stretched coordinates in the direction perpendicular to the coast such that right at the coast $f\Delta x/c = 0.2$. We find on average over 200 time steps that:

—the discrepancy between the numerical and analytical plateau value of the interface displacement (see Fig. 6) is less than 1%;

—the numerical wave speed evaluated from the most southern Kelvin wave front (see Fig. 6) differs by less than 2% from the exact value; and

—numerical values of velocities along the coast $x = 0$ differ by less than 2% from their analytical values.

4. Discussion

We have developed a scheme, free of two-grid oscillations, that appears suitable for coastal and semi-enclosed basins circulation problems that can be modelled by the two-layer shallow water equations. The flexibility of triangular elements allows a more homogeneous grid than quadrilateral elements in the case of a complicated geometry. The importance of a homogeneous grid should be kept in mind for problems involving wave propagation, in order to avoid false refraction and reflection due to the grid.

Although we have not performed direct comparisons with finite difference methods, we think that for simple geometries such as square boxes the above scheme should not be used, because of the penalizing storage space needed. However, for problems involving complicated geometries and for cases where boundary conditions should be incorporated as exactly as possible, the scheme presented here is relevant.

In our case, using a semi-implicit time marching scheme, the alliance of linear non-conforming elements for velocity variables and linear con-

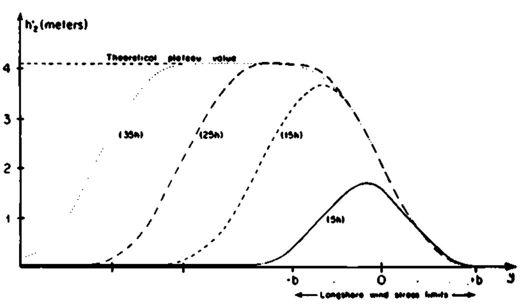

Fig. 6. Interface displacement h_2' at the coast $x = 0$, at different times.

forming elements for height variables, present the following advantages over using conforming elements for both variables, associated with "mass lumping": (i) the scheme is completely free of two-grid oscillation problems; (ii) the analytical elimination of velocities yields an exact discrete system of equations for water heights with an easily implemented structure; and (iii) the boundary condition of no normal flux is straightforward to handle.

5. Acknowledgement

This work was supported by R. C. P. 613: "Modelisation des écoulements océaniques" of the Centre National de la Recherche Scientifique.

REFERENCES

Allen, J. S. 1976. Some aspects of the forces wave response of stratified coastal regions. *J. Phys. Oceanogr. 6*, 113–119.

Arakawa, A. and Lamb, V. R. 1981. A potential enstrophy and energy conserving scheme for the shallow water equations. *Mon. Wea. Rev. 109*, 18–36.

Crepon, M. and Richez, C. 1982. Transient upwelling generated by two-dimensional atmospheric forcing and variability of the coastline. *J. Phys. Oceanogr. 12*, 1437–1457.

Hua, B. L. and Thomasset, F. 1983. A numerical study of the effects of coastline geometry on wind-induced upwellings in the Gulf of Lions. *J. Phys. Oceanogr. 13*, 678–694.

Hurlburt, H. E. and O'Brien, J. J. 1972. A numerical model of coastal upwelling. *J. Phys. Oceanogr. 2*, 14–26.

Kwizack, M. and Robert, A. J. 1971. A semi-implicit scheme for grid point atmospheric models of the primitive equations. *Mon. Wea. Rev. 99*, 32–36.

Mesinger, F. 1973. A method for construction of second order accuracy difference schemes permitting no false two-grid interval wave in the height field. *Tellus 25*, 444–458.

Pinder, G. F. and Gray, W. G. 1977. *Finite elements simulation in surface and subsurface hydrology*. New York: Academic Press.

Platzmann, G. W. 1981. Some response characteristics of finite element tidal model. *J. Comp. Phys. 40*, 36–63.

Schoenstadt, A. L., 1980. A transfer function analysis of numerical schemes used to simulate geostrophic adjustment. *Mon. Wea. Rev. 108*, 1248–1259.

Thomasset, F. 1981. *Implementation of finite elements methods for Navier–Stokes equations*. Springer Verlag: Berlin.

Williams, R. T. 1981. On the formulation of finite-element prediction models. *Mon. Wea. Rev. 109*, 463–466.

Zienkiewicz, O. C., 1977. *The finite element method in engineering science*. McGraw-Hill: New York.